Investigate the height dependency of the micro-/defect-structure and mechanical properties of additively manufactured AlF357 aluminum alloy

Md Faysal Khan[1,2], P.D. Nezhadfar[1,2], Paul R. Gradl[3], Donald Godfrey[4], Jacky Diemann[5], Shuai Shao[1,2], Nima Shamsaei[1,2*]

[1]National Center for Additive Manufacturing Excellence (NCAME), Auburn University, Auburn, AL 36849, USA

[2]Department of Mechanical Engineering, Auburn University, Auburn, AL 36849, USA

[3]Propulsion Department, NASA Marshall Space Flight Center, Huntsville, Al 35812, USA

[4]SLM Solutions NA, Inc. Wixom, MI 48393, USA

[5]SLM Solutions Group AG, Lübeck, Germany

* Corresponding author:

Email: shamsaei@auburn.edu

Tel: (334) 844 4839

Abstract

When the laser powder bed fusion (L-PBF) additive manufacturing method is employed to build parts with increased heights, there is a possibility that defects are increased in part. This study investigates the effect of build height on the micro-/defect-structure and, consequently, the mechanical properties of L-PBF AlF357, an Al-Si-Mg alloy family. Tall vertical cylinders of 316 mm with 15 mm diameter were fabricated and cut into specimens at different heights. Although not much difference is observed in the microstructure (grain size and morphology), the defects' size and population slightly vary with height. Nonetheless, the tensile properties of the L-PBF AlF357 are found to be independent of height. This is ascribed to the approximately identical microstructure and marginal difference in the defect's size and distribution along the heights.

Keywords: Laser powder bed fusion (L-PBF), AlF357, Height dependency, Microstructure, Porosity, Tensile properties

Introduction

Additive manufacturing (AM), a layer-by-layer process, bypasses geometric constraints while constructing the desired parts based on computer-aided design (CAD) [1]. AM enables cost-effective production; tailoring materials' properties often exhibit superior to the conventionally manufactured (CM) counterparts [2,3]. Laser powder bed fusion (L-PBF) is one of the well-established AM technologies in which a pre-alloyed powder is distributed over the bed. A high-

power-density laser melts and fuses powder particles to create the parts [4,5]. The rapid solidification in L-PBF could significantly refine the microstructure and sometimes improve the material's tensile and fatigue performance [6]. The parts are being designed and manufactured in new ways because of different AM processes. Unlike conventionally manufactured materials, the local geometries and microstructure of AM materials can change across short distances.

Aluminum (Al) alloys are the most widely used metal after steel, titanium alloys. The Al alloys are classified into cast, wrought, etc. But the AM processes have many advantages, e.g., finer microstructure, short production cycle, low cost, good flexibility, geometrical accuracy complexity etc. The current demand to produce geometrically complex, lightweight, corrosion-resistant, high thermal conductive Al alloys have been investigated continuously by the different AM processes for the applications in aerospace, defense, automotive, naval industries, and various structural components [7].

The most common aluminum alloys, which have been studied extensively, are AlSi10Mg [8,9], AlSi12 [10,11] and AlSi7Mg [12,13]. Among these, AlSi7Mg is a widely used casting aluminum alloy with a composition near the eutectic point and high Si content. Recently, the most popular AlSi7Mg fabricated by the L-PBF method are A356, A357, and F357. A member of the Al-Si-Mg casting alloy family (particularly alloy F357 [14], a beryllium-free variant of A357), which possesses exceptional fluidity and castability [15], is especially appealing out of the beryllium-related health concerns of its Axxx series counterpart.

Several investigations have revealed local property variation in several AM materials as a function of build orientation and height. A variogram analysis is utilized by R.K. Everett et al. [16] to demonstrate the auto-correlation of grain sizes and tensile properties with build height in the L-PBF AlSi10Mg parts. The results showed that the local geometries and build heights, even at constant process parameters, affect the grain size and tensile properties of L-PBF AlSi10Mg. The investigation of the build height effect on L-PBF IN718 showed no significant changes in mechanical properties along with the build height of the parts. However, there were some differences in the grain structures [17]. G. Mohr et al. [18] investigated the effects of inter-layer time (ILT) and build height on the grain size, melt pool, and hardness of 316L stainless steel. They found a significant impact of ITL and build height on heat accumulation and, in turn, on microstructure and hardness.

A few studies investigated the effect of build height variation with different alloys and the change in process parameters, local geometries, etc. But there is no study on Al alloys' build height dependency, specifically AlF357 on micro-/defect-structure and tensile properties. This study investigates the effect of the build height on the microstructure, defect structure, and tensile properties of tall L-PBF AlF357 aluminum parts.

Experimental Procedure

Material and Fabrication

The AlF357 virgin pre-alloyed powder supplied by IMR Metal Powder Technologies GmbH with the powder particle size in the range of 20-63 μm in compliance with SAE AMS 4289 standard [19] was used in this study. An SLM280 2.0 machine, an L-PBF platform, was used to fabricate all the specimens. The chemical composition of the AlF357 powder is listed in **Table 1**.

Table 1. Chemical composition of AlF357 powder, provided by IMR Metal Technologies.

	Si	**Mg**	**Fe**	**Cu**	**Mn**	**Ti**	**Zn**	**Pb**	**Ni**	**V**
(wt. %)	7.10	0.56	0.078	0.001	0.001	0.07	0.002	0.001	0.003	0.008
	Zr	**O**	**H**	**N**	**Al**					
(wt. %)	0.001	0.019	0.002	<0.002	Bal					

Argon gas was used as the shielding gas during fabrication to protect the melt pool from oxidation and mitigate spatter. The process parameters used to fabricate the specimens are listed in **Table 2**.

Table 2. Process parameters used for fabricating the L-PBF AlF357, provided by SLM Solutions.

Laser power (W)	Scan speed (mm/s)	Hatch distance (mm)	Layer thickness (μm)
370	1225	0.10	30

Tall cylindrical rods with a diameter of 15 mm and a length of 316 mm were fabricated (see **Figure 1 (a)**). A tall cylindrical bar was then cut into four specimens with equal length (79 mm) for micro-/defect-structure characterization; they were designated as Bottom, Middle 1, Middle 2, and Top specimens along the build direction. For tensile tests, the cylindrical bars were cut into three specimens: Bottom, Middle, and Top. Finally, the cut specimens were further machined to the final geometry of the tensile specimens with uniform gage sections following ASTM E08 [20]. The geometry of the tensile specimen is presented in Figure 1 (b). All the specimens in this study are non-heat treated (NHT).

Micro-/defect-structure characterization

The microstructure characterizations were conducted in both the transverse direction (TD) plane, i.e., parallel to the build direction, and the normal direction (ND) plane, i.e., perpendicular to the build direction. The specimens were cut accordingly, cold-mounted, ground with sandpapers with grits ranging from 320 (grain size of 46.3 μm) to 4000 (grain size of 5 μm), and polished to a mirror-finished surface. Electron backscatter diffraction (EBSD) and electron channeling contrast imaging (ECCI) were conducted for microstructure characterization using a Zeiss

Crossbeam 550 scanning electron microscope (SEM). The chemical analysis was carried out via the electron dispersive spectroscopy (EDS) method by an Oxford detector attached to the SEM.

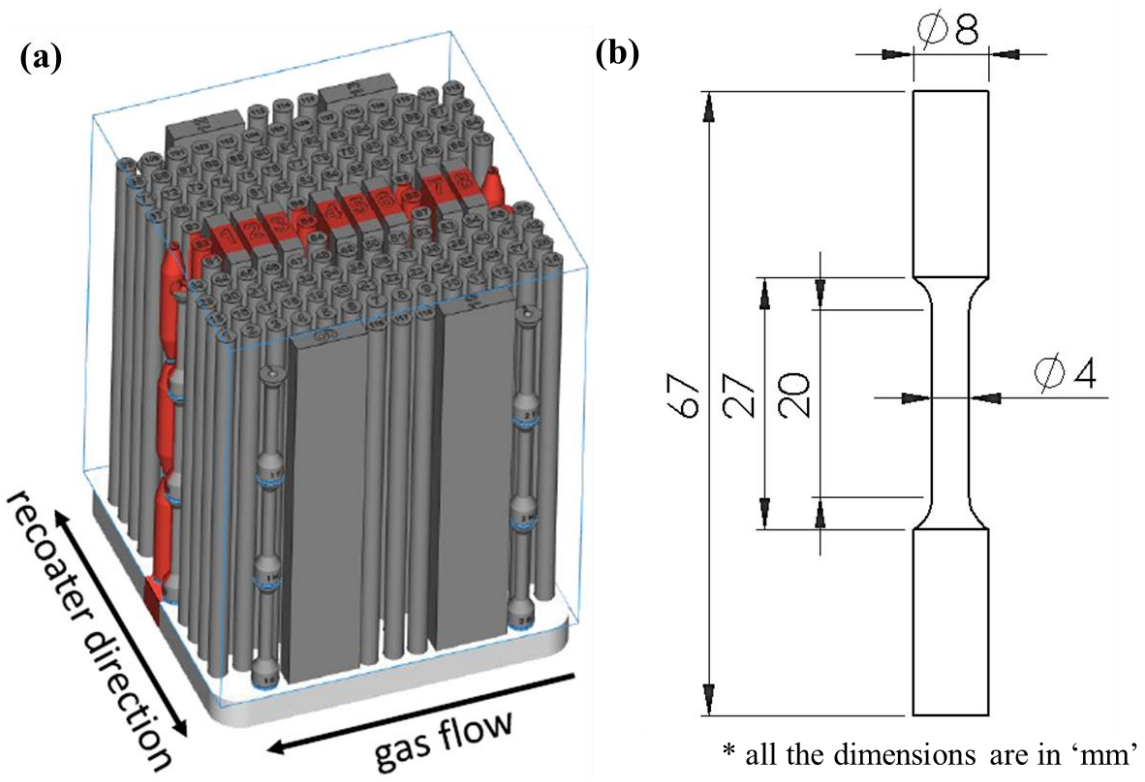

Figure 1. (a) The build layout, showing different types of parts fabricated (Note that only cylindrical bars are being investigated in this study), (b) the geometry of the tensile specimens following ASTM E08 [20].

To characterize the defect structure of the specimens, an X-ray CT scan was conducted on the specimens using a Zeiss Xradia 620 Versa system. The voltage and power were 80 kV and 7 W, respectively, for each scan with a voxel size of 5.0 µm. The raw X-CT files were reconstructed using a Zeiss proprietary software. The 3D visualization and statistical results of the scans were extracted to compare the defect levels at different heights.

Mechanical testing

The tensile tests were performed using an MTS landmark servo-hydraulic load frame with a load cell of 100 kN. The quasi-static tensile tests were conducted in two steps: a strain-controlled step up to ~0.035 mm/mm strain followed by a displacement-controlled step. An MTS mechanical extensometer was attached to the specimen in the gage section to record the strain. The tensile tests were repeated three times for each of the heights to check the repeatability of the results.

Results and Discussion

Microstructure analysis

The microstructures of the L-PBF AlF357 specimens at four different heights, Bottom, Middle 1, Middle 2, and Top, in non-heat treated (NHT) condition are presented in **Figure 2**. The inverse pole figure (IPF) maps obtained from EBSD analysis on the TD and ND planes. The grain morphology is found almost similar at different heights, columnar grains on the TD plane and equiaxed on the ND plane. The mean grain size on the TD plane along the different heights are found similar; from bottom to top, the mean grain size is 7.8 ± 5.6 µm, 8.6 ± 5.8 µm, 8,1 ± 5.7 µm, and 8.2 ± 5.6 µm, respectively (see **Figures 2** (a) (c) (e) (g)). The texture is also remained identical along the build heights without much variation. On the ND plane, the mean grain size is also very similar along the heights, and from bottom to top, are found to be 6.5 ± 3.2 µm, 7.1 ± 3.8 µm, 6.9 ± 3.8 µm, and 6.5 ± 3.2 µm, respectively. The texture is almost constant on the ND planes along the build height.

Among the microstructures presented in **Figure 2**, there is no significant change in grain structure, texture, and mean grain size along with the height of the specimens. **Figure 3** shows the BSE micrographs of L-PBF AlF357 on the TD plane along the different build heights. The Si-element maps obtained by EDS analysis are also presented in **Figure 3**. There are some changes in Si-networks in **Figure 3** along the different heights, mainly because of thermal gradients. In the bottom, the cellular structures are more dendritic but moving along the heights, the dendritic microstructure becomes finer. But in the top, the cellular structure is growing. These dendritic structures at the bottom may be because of its closeness to the built plate, and heat dissipation is faster at that part, but in the higher part, the specimens are already in the powder, and the thermal gradient is also lower, so it remains hot for a period of time. Therefore, the dendritic structures try to reform and become finer. However, on the top these dendritic structures are growing.

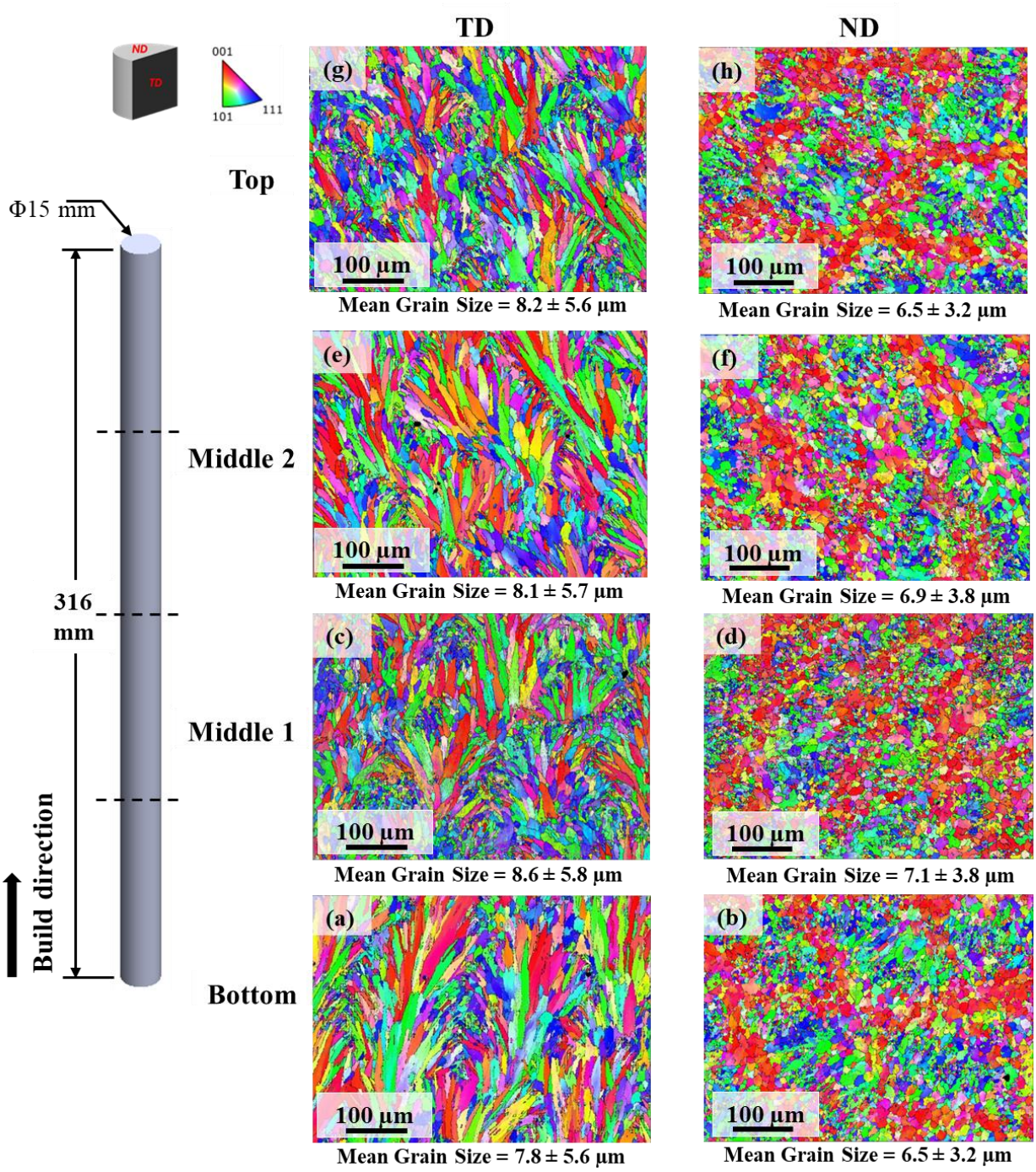

Figure 2. Inverse pole figure (IPF) maps obtained by EBSD along the TD plane, parallel to the build direction and the ND plane, perpendicular to the build direction, for the L-PBF AlF357 at four different heights in NHT conditions; (a-b) bottom, (c-d) middle 1, (e-f) middle 2, and (g-h) top.

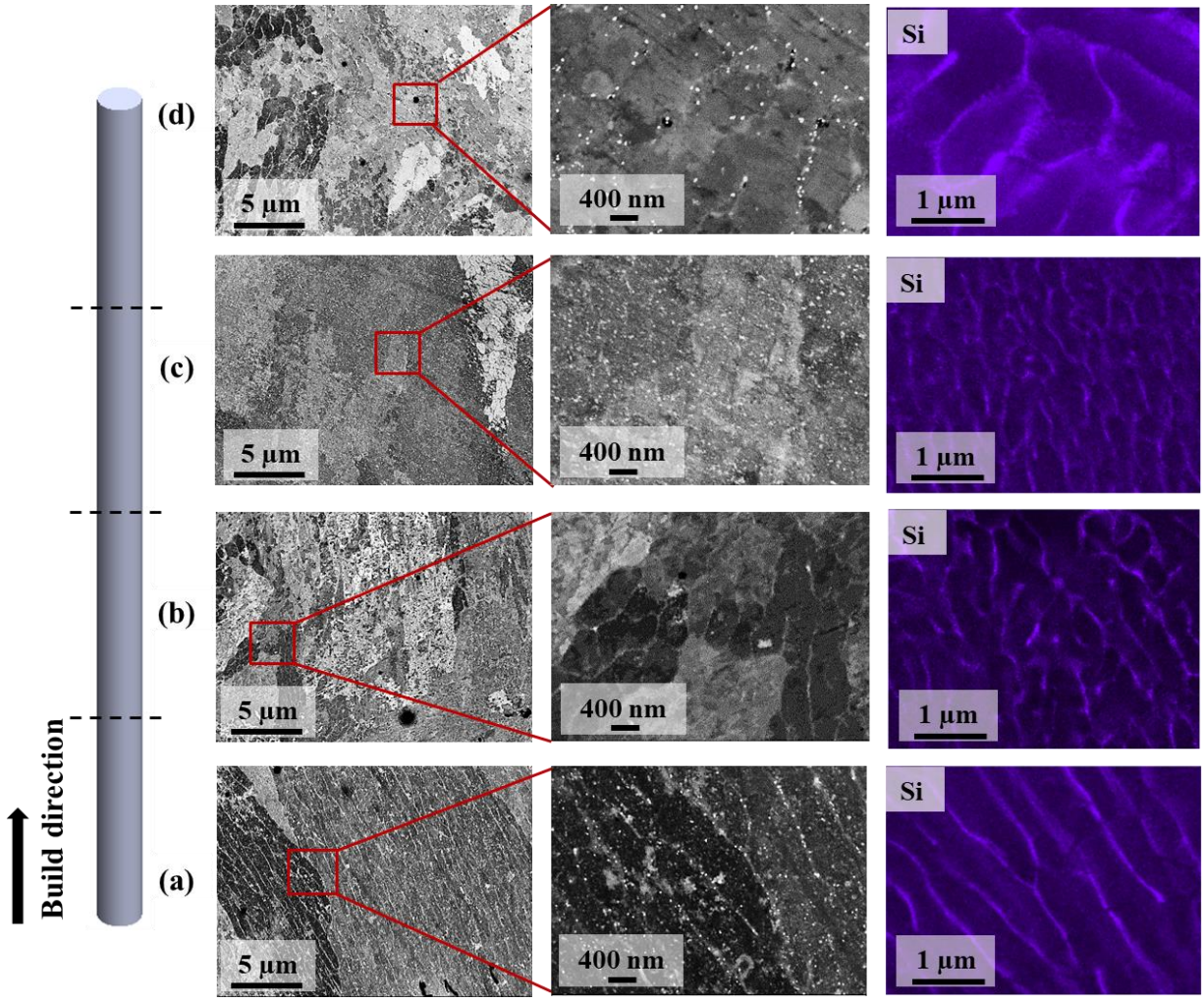

Figure 3. BSE micrographs of L-PBF AlF357 along the transverse direction (TD) parallel to the build direction at four different heights in NHT conditions showing the dendritic microstructure; (a) bottom, (b) middle 1, (c) middle 3, and (d) top along with the Si element maps by EDS.

Defect-structure analysis

The X-CT results from the gage section of the tensile specimens in the NHT condition are presented in **Figure 4(a-c)**, along with the build height. Also, the defect size distributions are shown in **Figure 4(d)**, comparing the porosity count per unit volume (mm^{-3}) for different heights. There are variations in the size and distribution of porosity along the build heights, and the overall porosity density is also changing significantly (see **Figure 4(e)**). Because of optimized process parameters that have been used for the fabrication of L-PBF AlF357, a moderate defect density is observed in as-built specimens. However, the defect density gradually increased, moving along the built direction to the middle and top. The thermal gradient, high thermal conductivity, and relative position from the built plate might be contributed to this. In contrast, the heated built plate acts as heat treatment for the bottom specimen, increasing the porosity [21]. And along the build

direction, going further away from the built plate decreased the number of total porosity counts per volume. Still, larger pore formation increased because of the high thermal conductivity of this alloy [15].

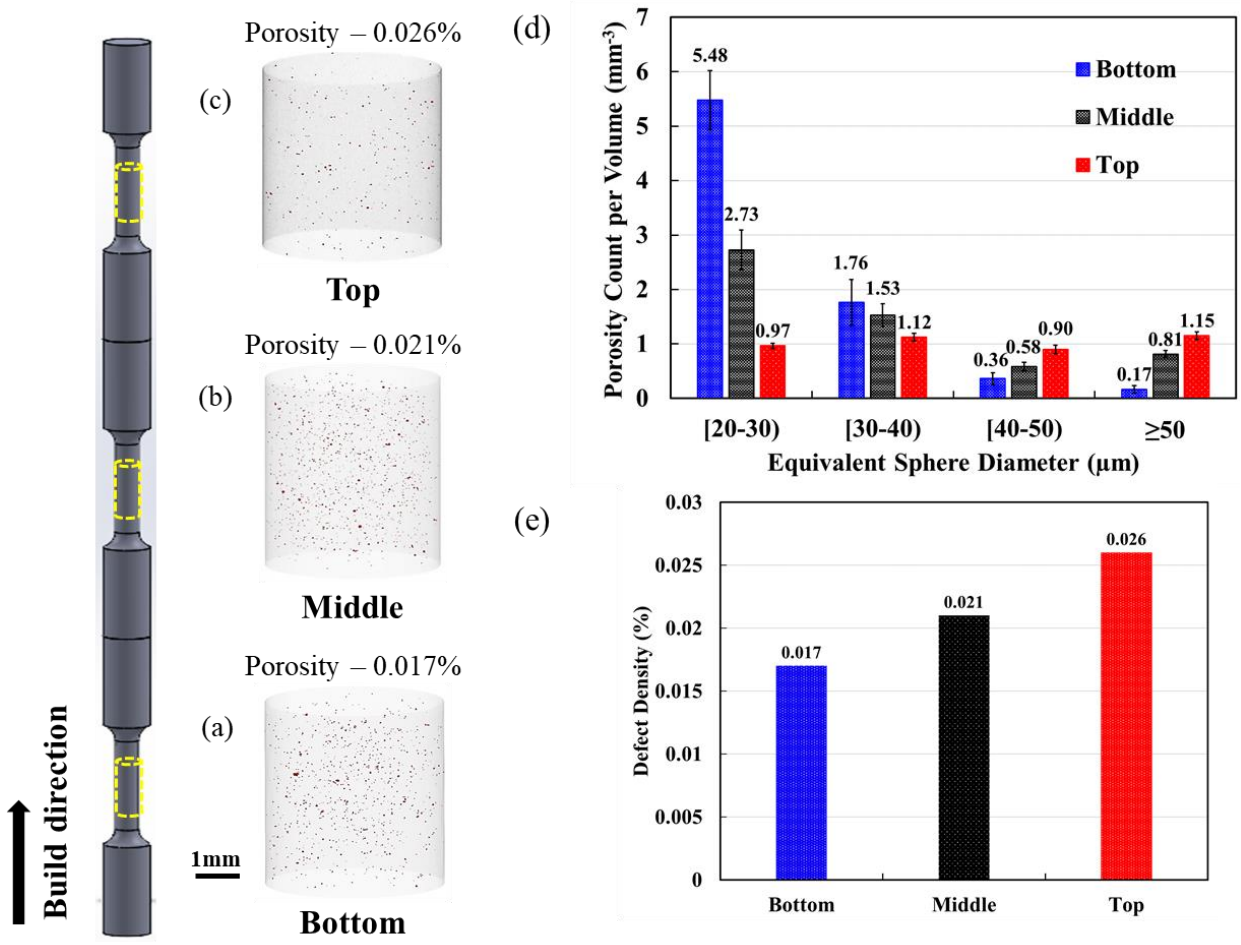

Figure 4. X-ray CT scan results for the (a) bottom, (b) middle, and (c) top of the L-PBF AlF357 specimen in NHT condition. (d) Porosity size distributions of L-PBF AlF357 specimens from different heights. The statistical results are shown in (e).

Tensile properties

The quasi-static tensile properties, i.e., yield strength (YS), ultimate tensile strength (UTS), and percent elongation (%EL), of NHT L-PBF AlF357 specimens along the build height are presented in **Figure 5**. As seen, the tensile properties are almost similar along the build height showing static properties height independency of L-PBF AlF357. This may be attributed to specimens' similar microstructure (grain morphology, size) at different heights. Guo et al. [22] showed the change in tensile properties is attributed to the change in microstructures.

The porosity level influences tensile properties especially ductility; it has been shown that the ductility can be increased by decreasing the volumetric defects. Although the size and the

defect density increase along the heights (see **Figure 4**), these are not too influential on the tensile properties of L-PBF AlF357 specimens resulting in almost comparable %EL along with the build height [23].

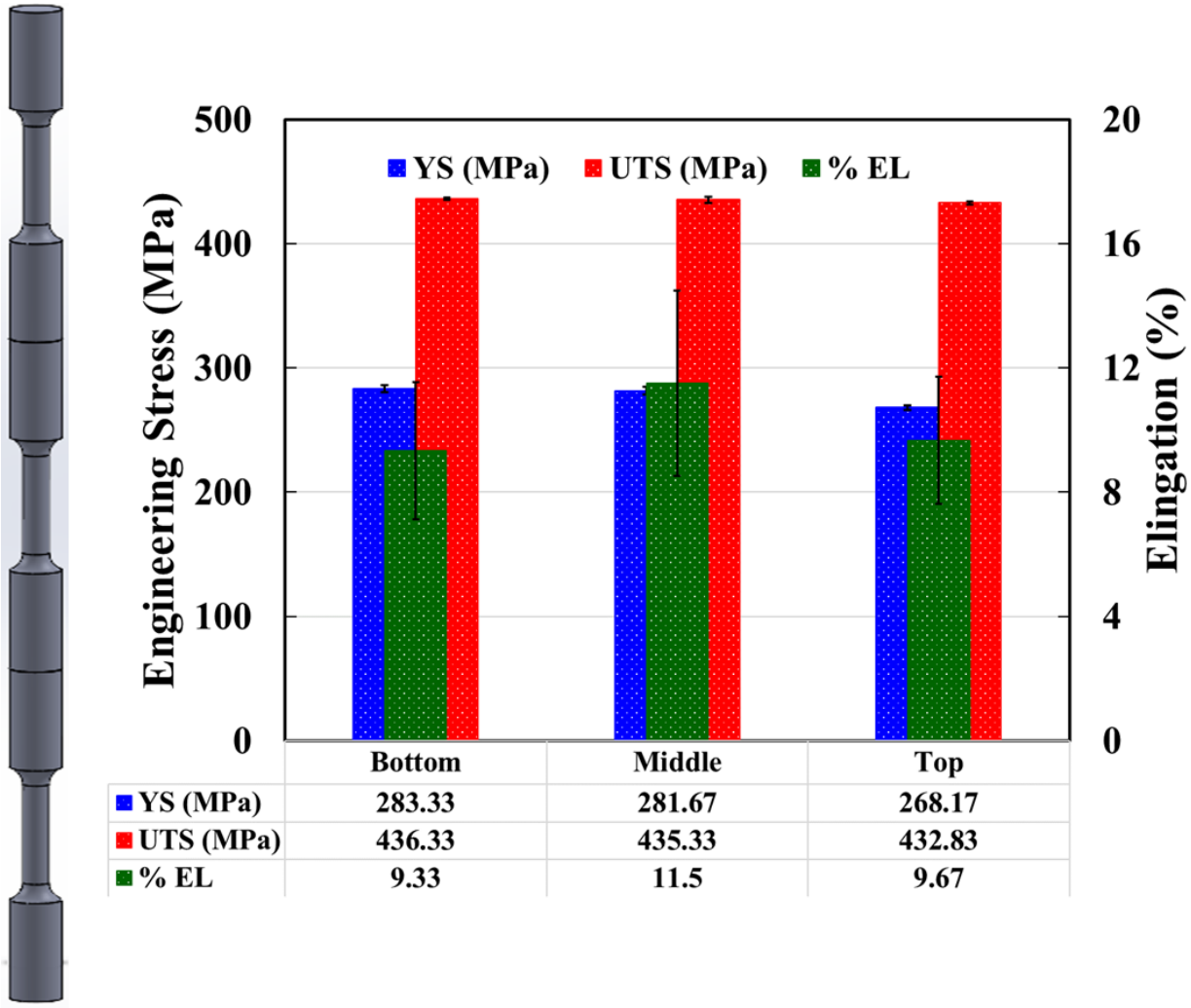

Figure 5. Bar chart representation of the tensile properties of L-PBF AlF357 alloy with different heights.

Conclusions

This study compared the microstructures, defects, and tensile properties of tall L-PBF AlF357 alloys along the different build heights in the non-heat-treated condition. The effects of

microstructure and defects on the tensile properties were investigated along the build heights, and the findings are concluded as follows:

1. There was no height dependency of microstructure seen for the L-PBF AlF357; the microstructure was similar along the build heights in both transverse direction (TD) and normal direction (ND) planes. The grains were columnar in the TD plane and were equiaxed in the ND plane. There were no significant changes in average grain size at the different heights of the L-PBF AlF357.
2. There was a change in defect content observed along the build heights for the L-PBF AlF357. The population of the defects per unit volume is decreasing, and the size of the defects is increasing along the heights.
3. Since there are no significant changes in microstructure along the different build heights, the tensile properties (strength and ductility) are also similar. However, some defect size and population changes did not influence the tensile properties.

Acknowledgment

This research is partially supported by the National Aeronautics and Space Administration NASA under Cooperative Agreement No. 80MSFC19C0010. This material is also based upon work partially supported by the National Science Foundation (NSF) under grant No. 1919818. This paper describes objective technical results and analysis. Any subjective views or opinions that might be expressed in the paper do not necessarily represent the views of the National Aeronautics and Space Administration (NASA) or the United States Government.

References

[1] ASTM International. ASTM52900-15 standard terminology for additive manufacturing—general principles—terminology. West Conshohocken, PA 19428-2959 USA 2015;3:5.

[2] Calignano F. Investigation of the accuracy and roughness in the laser powder bed fusion process. Virtual Phys Prototyp 2018;13:97–104. https://doi.org/10.1080/17452759.2018.1426368.

[3] Sing SL, An J, Yeong WY, Wiria FE. Laser and electron-beam powder-bed additive manufacturing of metallic implants: A review on processes, materials and designs. J Orthop Res 2016;34:369–85. https://doi.org/https://doi.org/10.1002/jor.23075.

[4] Otani Y, Sasaki S. Effects of the addition of silicon to 7075 aluminum alloy on microstructure, mechanical properties, and selective laser melting processability. Mater Sci Eng A 2020;777:139079. https://doi.org/https://doi.org/10.1016/j.msea.2020.139079.

[5] Bremen S, Meiners W, Diatlov A. Selective Laser Melting. Laser Tech J 2012;9:33–8. https://doi.org/https://doi.org/10.1002/latj.201290018.

[6] Prashanth KG, Scudino S, Eckert J. Defining the tensile properties of Al-12Si parts produced by selective laser melting. Acta Mater 2017;126:25–35.

https://doi.org/https://doi.org/10.1016/j.actamat.2016.12.044.

[7] Olakanmi EO, Cochrane RF, Dalgarno KW. A review on selective laser sintering/melting (SLS/SLM) of aluminium alloy powders: Processing, microstructure, and properties. Prog Mater Sci 2015;74:401–77. https://doi.org/https://doi.org/10.1016/j.pmatsci.2015.03.002.

[8] Paul MJ, Liu Q, Best JP, Li X, Kruzic JJ, Ramamurty U, et al. Fracture resistance of AlSi10Mg fabricated by laser powder bed fusion. Acta Mater 2021;211:116869. https://doi.org/https://doi.org/10.1016/j.actamat.2021.116869.

[9] Muhammad M, Nezhadfar PD, Thompson S, Saharan A, Phan N, Shamsaei N. A comparative investigation on the microstructure and mechanical properties of additively manufactured aluminum alloys. Int J Fatigue 2021;146:106165. https://doi.org/https://doi.org/10.1016/j.ijfatigue.2021.106165.

[10] Ponnusamy P, Masood SH, Ruan D, Palanisamy S. Effect of build orientation and elevated temperature on microhardness and deformation of dynamically tested SLM processed AlSi12 alloy. Mater Today Proc 2021;38:2488–92. https://doi.org/https://doi.org/10.1016/j.matpr.2020.07.514.

[11] Siddique S, Imran M, Wycisk E, Emmelmann C, Walther F. Influence of process-induced microstructure and imperfections on mechanical properties of AlSi12 processed by selective laser melting. J Mater Process Technol 2015;221:205–13. https://doi.org/https://doi.org/10.1016/j.jmatprotec.2015.02.023.

[12] Asghar G, Peng L, Fu P, Yuan L, Liu Y. Role of Mg2Si precipitates size in determining the ductility of A357 cast alloy. Mater Des 2020;186:108280. https://doi.org/https://doi.org/10.1016/j.matdes.2019.108280.

[13] Casati R, Vedani M. Aging Response of an A357 Al Alloy Processed by Selective Laser Melting. Adv Eng Mater 2019;21:1800406. https://doi.org/https://doi.org/10.1002/adem.201800406.

[14] EOS. Material Data Sheet EOS Aluminium AlF357 Light Weight & Corrosion resistance. 2019.

[15] Nezhadfar PD, Thompson S, Saharan A, Phan N, Shamsaei N. Structural integrity of additively manufactured aluminum alloys: Effects of build orientation on microstructure, porosity, and fatigue behavior. Addit Manuf 2021;47:102292. https://doi.org/https://doi.org/10.1016/j.addma.2021.102292.

[16] Everett RK, Duffy ME, Storck SM, Zupan M. A Variogram Analysis of Build Height Effects in an Additively Manufactured AlSi10Mg Part. Addit Manuf 2020;35:101306. https://doi.org/https://doi.org/10.1016/j.addma.2020.101306.

[17] Wang X, Keya T, Chou K. Build Height Effect on the Inconel 718 Parts Fabricated by Selective Laser Melting. Procedia Manuf 2016;5:1006–17. https://doi.org/https://doi.org/10.1016/j.promfg.2016.08.089.

[18] Mohr G, Altenburg SJ, Hilgenberg K. Effects of inter layer time and build height on resulting properties of 316L stainless steel processed by laser powder bed fusion. Addit Manuf 2020;32:101080. https://doi.org/https://doi.org/10.1016/j.addma.2020.101080.

[19] SAE International. AMS4289 Aluminum Alloy Castings 7.0Si - 0.55Mg - 0.12Ti (F357.0-T6) Solution and Precipitation Heat Treated. AMS D Nonferrous Alloy Comm 2013. https://doi.org/https://doi.org/10.4271/AMS4289.

[20] ASTM International. ASTM E8/E8M standard test methods for tension testing of metallic materials. West Conshohocken, PA 19428-2959 USA 2013. https://doi.org/10.1520/E0008.

[21] Defanti S, Bassoli E. Repeatability of the fatigue performance of additively manufactured A357.0 under different thermal treatment conditions. Mater Sci Eng A 2021;805:140594. https://doi.org/https://doi.org/10.1016/j.msea.2020.140594.

[22] Guo M, Sun M, Huang J, Pang S. A Comparative Study on the Microstructures and Mechanical Properties of Al-10Si-0.5Mg Alloys Prepared under Different Conditions. Metals (Basel) 2022;12. https://doi.org/10.3390/met12010142.

[23] Nezhadfar PD, Shamsaei N, Phan N. Enhancing ductility and fatigue strength of additively manufactured metallic materials by preheating the build platform. Fatigue Fract Eng Mater Struct 2021;44:257–70. https://doi.org/10.1111/ffe.13372.